Clin Neuroradiol (2019) 29:533–541
https://doi.org/10.1007/s00062-018-0682-4

ORIGINAL ARTICLE

Cerebral Perforating Artery Disease

Characteristics on High-Resolution Magnetic Resonance Imaging

Jianye Liang[1] · Yiyong Liu[1] · Xiaoshuang Xu[1] · Changzheng Shi[1] · Liangping Luo[1]

Received: 12 December 2017 / Accepted: 7 March 2018 / Published online: 23 March 2018

Abstract

Purpose Our aims were to evaluate the feasibility of high-resolution magnetic resonance imaging (HR-MRI) for displaying the cerebral perforating arteries in normal subjects and to discuss the value of HR-MRI for detecting the causes of infarctions in the territory of the lenticulostriate artery (LSA).

Methods Included in this study were 31 healthy subjects and 28 patients who had infarctions in the territory supplied by the LSA. The T1-weighted imaging (T1WI), T2WI, diffusion-weighted imaging (DWI), and HR-MRI, including 3-dimensional time-of-flight magnetic resonance angiography (3D-TOF-MRA) and 3D fast spin-echo T1WI (namely CUBE T1 in GE Healthcare), were applied on a 3-Tesla scanner. The numbers and route of the perforating arteries on both sides were independently confirmed on HR-MRI by two physicians. The Wilcoxon test was used to compare the differences.

Results The numbers of perforating arteries in healthy subjects observed on 3D-TOF-MRA were as follows: numbers of the bilateral recurrent artery of Heubner (RAH) ranged from 0–3 (median 1), numbers of the left LSA ranged from 0–7 (median 3), numbers of the right LSA ranged from 0–5 (median 3), numbers of the bilateral anterior choroidal artery ranged from 1–2 (median 1) and the numbers of the bilateral thalamoperforating artery ranged from 1–2 (median 1). In the patients with lenticulostriate infarctions, the numbers of LSAs on the affected side were lower than on the opposite and ipsilateral sides in the healthy subjects. The results were statistically significant. An abnormality of the RAH may lead to a centrum semiovale infarct pattern, whereas an abnormality of the LSA is associated with a corona radiata infarct pattern.

Conclusion The use of HR 3D-TOF-MRA and CUBE T1 had unique advantages in displaying the tiny perforating arteries in vivo. Moreover, effective recognition of the associated cerebral perforating artery and infarct patterns may enhance our understanding of the mechanism of stroke in patients with lenticulostriate infarctions.

Keywords Infarct pattern · Magnetic resonance angiography · Fast spin-echo · Stroke mechanism · Lenticulostriate infarction

Introduction

Stroke is the second leading cause of death globally, with two thirds of cases occurring in developing countries, particularly in China [1]. The condition is associated with high morbidity, mortality, and disability. An early diagnosis and timely treatment significantly improves the prognosis of affected patients. Currently, standard imaging techniques exist to diagnose stroke early and accurately; however, in many clinical cases, no stenosis or occlusion of the large arteries that supply the territory of the infarction can be found using traditional angiography. Because of a previous inability to image tiny vessels, there are limited studies concentrating on this aspect of perforating artery disease, which is an important mechanism of stroke. Caplan et al. [2] reported that the incidence of acute cerebral infarction in the territory supplied by the lenticulostriate arteries (LSA) and paracentral arteries was approximately 39.5%, significantly higher than that of the atherosclerotic group (33.1%) and the lacu-

Jianye Liang, Yiyong Liu contributed equally to this work.

✉ Changzheng Shi
tsczcn@jnu.edu.cn

✉ Liangping Luo
tluolp@jnu.edu.cn

[1] Medical Imaging Center, The First Affiliated Hospital, Jinan University, Guangzhou, China

nar infarction group (27.4%) in Asia. The LSA is a terminal artery without any collateral branches; in contrast, it arises vertically from the middle cerebral artery (MCA), which renders the territory supplied by the LSA more susceptible to ischemia and leads to a high risk of arteriolar necrosis [3]. Although some cerebral perforating arteries have been confirmed anatomically, whether they can be detected and visualized in vivo using magnetic resonance imaging (MRI) remains unclear. With the development of other imaging techniques, there are two high-resolution sequences of MRI that show promise in this field of research [4]. High-resolution, three-dimensional, time-of-flight magnetic resonance angiography (HR 3D-TOF-MRA) is an improved bright blood imaging method using the propeller k-space filling and parallel acquisition techniques with tiny thickness and overlapping spacing for its high-resolution operation [5, 6]. The TOF-MRA is widely used in clinical applications for imaging the vessels without contrast agents [7]. The three-dimensional fast spin-echo T1-weighted imaging (namely CUBE T1 in GE Healthcare, Milwaukee, Wisconsin) is another black blood imaging method based on an ultra-long echo train length and a multiple flip angle (FA) sequence [8]. The volume data can be reconstructed in all directions with a high signal-to-noise ratio (SNR), contrast-to-noise ratio (CNR) and isotropic resolution. Compared with traditional computed tomography angiography (CTA) or MRA, these methods not only indicate the degree of arterial stenosis but also provide more information regarding atherosclerotic plaque formation, arterial dissection, vascular wall remodeling, and vasculitis [9–11]. In addition, the image resolution of the two technologies has reached the sub-millimeter level, making it possible to visualize the tiny cerebral perforating arteries in vivo.

In this study, we chose the LSA for investigation in the group of vessels involved in perforating artery disease because it has a relatively stable number of branches arising from the MCA. Moreover, the LSAs primarily supply important territories including the basal ganglia and internal capsule, which are vulnerable to ischemia and cause obvious clinical symptoms [12]. We initially investigated the feasibility of HR-MRA for visualizing the perforating artery in normal subjects. In addition, we explored the diagnostic value of HR-MRA in cerebral perforating artery disease by comparing the numbers of LSAs on the contralateral and ipsilateral sides in normal subjects. The recurrent artery of Heubner (RAH) and LSA are terminal arteries arising from different large arteries. They supply an overlapping territory in the basal ganglia. The infarct pattern may also help to distinguish the stroke mechanisms as it remains unclear in perforating artery disease. We divided the infarcts into corona radiata and centrum semiovale infarct patterns, according to the study of Wang and Wang [13] and compared the difference of infarct patterns between the culprit RAH and LSA.

Material and Methods

Participants

All the participants were consecutively enrolled in this prospective study from October 2016 to October 2017. In general, the participants were recruited primarily from the physical examination center, where they presented for annual physical check-ups. A total of 31 subjects were recruited for the healthy group, including 18 males and 13 females. The ages ranged from 7 to 65 years, and the median age was 28 years. The inclusion criteria were as follows: (1) no neurologically-related clinical symptoms or medical history and a negative clinical neurological examination, (2) no obvious abnormal signal in the brain on conventional MRI sequences, e. g., T1-weighted imaging (T1WI), T2WI, and diffusion weighted imaging (DWI) and (3) no related contraindications to magnetic resonance examination. This study was approved by the ethics committee of our hospital, and all the participants provided informed consent before MR examination.

We initially included 30 patients in the perforating artery disease group, 2 of which were ruled out because of obvious movement artifacts and 28 patients were eventually included in this group, including 18 males and 10 females. The ages ranged from 33 to 70 years, and the median age was 52 years. The inclusion criteria were as follows: (1) acute isolated infarcts occurring in the territory supplied by the LSA regardless of the lesion size and (2) less than 50% stenosis of the ipsilateral intracranial or extracranial large artery. The cardiovascular risk factor distribution and general baseline characteristics of both groups are listed in Table 1.

Imaging Protocol

The study was performed on a 3-Tesla scanner with an 8-channel head coil (MR750, GE Healthcare, Milwaukee, WI, USA). The conventional MR sequences that were performed included T1WI, T2WI, DWI, and HR sequences, including 3D-TOF-MRA and CUBE T1. The parameters of T1WI were set as follows: repetition time (TR) 1750 ms, echo time (TE) 25 ms, thickness 5 mm, spacing 1.5 mm, field of view (FOV) 24 × 18 cm, and matrix 320 × 256. The parameters of T2WI were set as follows: TR 6818 ms, TE 106 ms, thickness 5 mm, spacing 1.5 mm, FOV 24 × 18 cm, and matrix 512 × 512. The parameters of DWI were set as follows: TR 3000 ms, TE 71 ms, thickness 5 mm, spacing

Table 1 Cardiovascular risk factor distribution and general baseline characteristics of healthy group and perforating artery disease group

	Healthy group	Perforating artery disease group	*P*
Male	18 (58.1%)	18 (64.2%)	0.174
Hypertension	2 (6%)	9 (32.1%)	0.032
Diabetes	3 (9.7%)	6 (21.4%)	0.043
Dyslipidemia	4 (12.9%)	11 (39.3%)	0.016
Smoking history	7 (22.6%)	12 (42.9%)	0.037
Obesity	6 (19.4%)	7 (25.0%)	0.076
Blood glucose (mmol/l)	5.84 ± 0.16	6.02 ± 2.48	0.082
Total cholesterol (mmol/l)	5.64 ± 0.71	5.82 ± 0.96	0.037
Low-density lipoprotein (mmol/l)	2.46 ± 0.72	2.87 ± 0.43	0.045

Data are presented as number (percentage) or mean ± standard deviation.

1.5 mm, FOV 24 × 24 cm, and matrix 160 × 160. The HR 3D-TOF-MRA images were obtained using the following parameters: TR 21 ms, TE 3.1 ms, thickness 0.6 mm, spacing –0.3 mm, FOV 22 × 17.8 cm, and matrix 480 × 448. The CUBE T1 [8, 14] images were acquired in an oblique coronal plane with the following parameters: TR 800 ms, TE 16 ms, thickness 0.6 mm, spacing –0.3 mm, FOV 23 × 18 cm, and matrix 480 × 320, echo-train length (ETL) 24, phase acceleration 2, and initial/minimum FA, 130°/20°. We applied variable refocusing FAs for compensating the signal decay resulting from a long ETL, which was used to reduce the scanning time in a fast spin-echo sequence [14]. The techniques of propeller k-space filling, fat suppression, and parallel acceleration along the phase direction were also used in CUBE T1. The voxel size, which represented spatial resolution, was $0.48 \times 0.57 \times 0.60\,mm^3$. Nearly 200 slices covering both the anterior and posterior circulation were obtained in 6 min 32 s.

Image Analysis and Post-processing

The image quality was divided into three levels: the cases with image quality at level 1 and level 2 were included in this study. The standards of classification were as follows: level 1, high-definition images without motion artifacts, level 2, less clear images with mild motion artifacts, but still useful for diagnosis and level 3, poor image quality with obvious motion artifacts, although the vessels were obscure. The HR images were sent to an Advantage Workstation 4.5 for post-processing (GE Medical Systems, Milwaukee, WI, USA). Multiplanar reconstruction along the route of the vessels was applied to the CUBE T1 images. Moreover, multi-angle TOF-MRA was also reconstructed for better visualization of the tiny arteries. The number, route, and morphology of the perforating arteries were documented in healthy volunteers. The number, route, and relationship of the LSA with the infarcts were documented in the perforating artery disease group.

Statistical Analysis

The SPSS 13.0 statistical software package (Chicago, IL, USA) was used for the statistical analysis. Each quantitative index was expressed as a mean with standard deviation. We compared the numbers of perforating arteries between the left and right sides in the healthy group and the ipsilateral and contralateral sides in the disease group using the Wilcoxon paired test. The differences between the affected side in the patients and the ipsilateral side in the normal subjects were compared using the Wilcoxon rank sum test. We compared the difference in the infarct patterns between RAH and LSA using Fisher's exact text ($n < 40$) and $P < 0.05$ was considered statistically significant.

Results

Healthy Group

The image quality for all the healthy subjects was high and acceptable. The numbers of perforating arteries in the healthy subjects observed on 3D-TOF-MRA were as follows: the number of left LSAs ranged from 0–7 (median 3) and the number of right LSAs ranged from 0–5 (median 3) (Fig. 1). The number of bilateral RAHs, including the medial striate arteries (MSA) ranged from 0–3 (median 1) (Fig. 2), there were 9 cases (29.0%) on the left side and 12 cases (35.5%) on the right side that were not detected. The number of bilateral anterior choroidal arteries (ACA) ranged from 1–2 (median 1) (Fig. 2). The number of bilateral thalamoperforating arteries (TPA) ranged from 1–2 (median 1), there were 8 cases (25.8%) on the left side and 7 cases (22.6%) on the right side that were not detected. The perforating arteries travelled naturally. Other perforating arteries including the thalamotuberal artery, thalamogeniculate artery, medial posterior choroidal artery, and lateral posterior choroidal artery could not be clearly detected (the specific results are listed in Table 2).

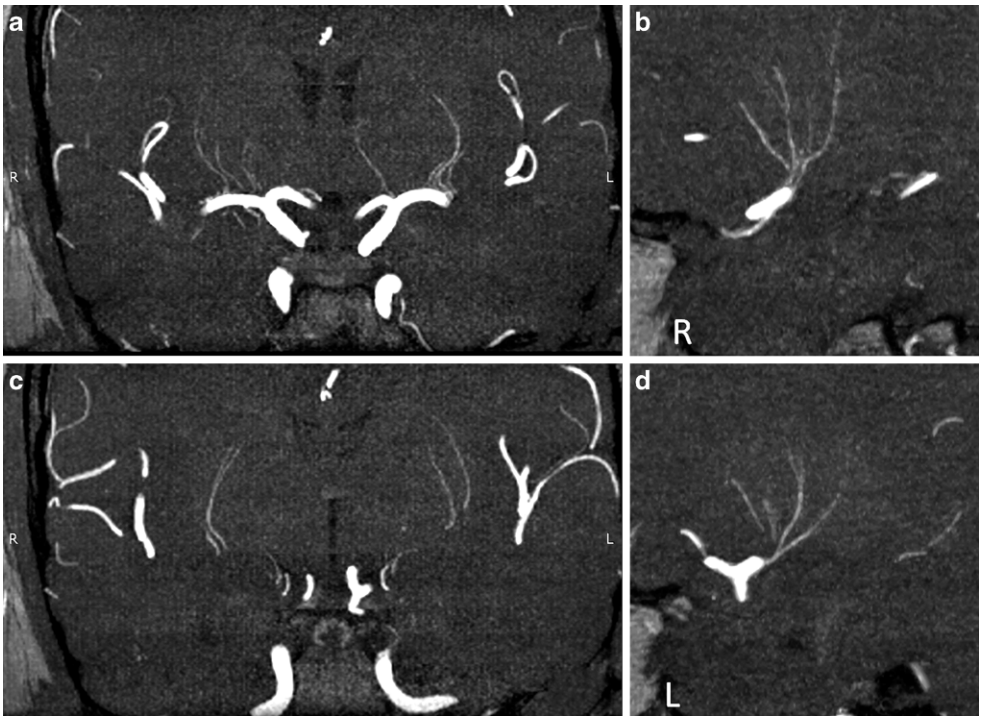

Fig. 1 Lenticulostriate arteries of normal subjects shown on HR 3D-TOF-MRA. The initial and distal segment of the lenticulostriate arteries travelled naturally with clear edges on coronal planes (**a**, **b**) and sagittal planes (**c**, **d**). They usually originated from the proximal segment of the middle cerebral artery

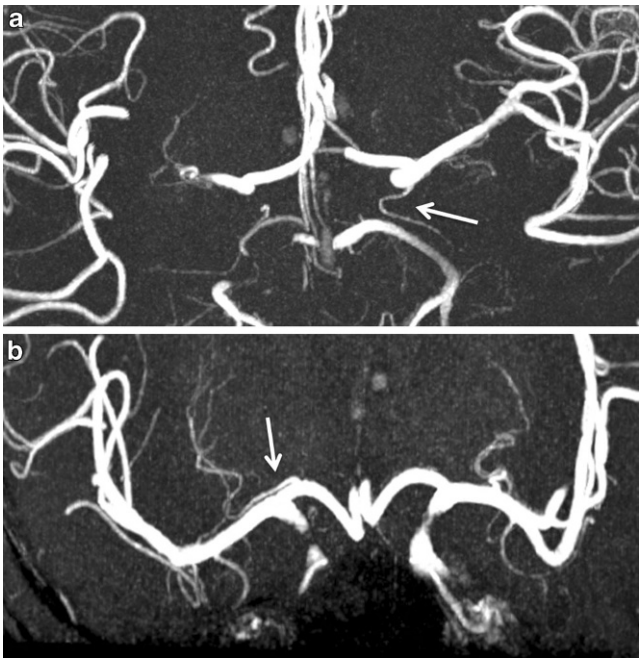

Fig. 2 Anterior choroidal artery and recurrent artery of Heubner, as shown on HR 3D-TOF-MRA. The anterior choroidal artery (*arrow*) generally originates from the supraclinoid segment of the internal carotid artery, close to the fork of the internal carotid artery (**a**). The recurrent artery of Heubner (*arrow*) usually originates from the A1 segment of the anterior cerebral artery (**b**)

The results of CUBE T1 showed that the number of left LSAs ranged from 0–5 (median 3) and the number of right LSAs ranged from 0–4 (median 3) (Table 3; Fig. 3).

Perforating Artery Disease Group

After excluding 2 patients for obvious motion artifacts, 28 patients were eventually included in the disease group. The severity of clinical symptoms varied depending on whether the capsula interna was involved. Of the patients 13 showed mild neurological symptoms, including impaired concentration, memory deterioration, dysphoria, slight headache, and dizziness; 9 patients showed moderate symptoms including facioplegia, dysphagia, dysarthria, hemianopsia, and somnolence and 6 patients showed severe symptoms including hemiplegia, hemidysesthesia and even coma. The time from symptom onset to image metrics (e.g., a high signal on DWI) ranged from 6 h to 4 days among the included patients, with a median time of 1 day. Among the patients with right-sided lenticulostriate infarctions, the numbers of LSAs on the right side ranged from 0–5 (median 2) and the numbers of LSAs on the left side ranged from 1–6 (median 3). For the number of LSAs on the right side, there were 2 cases of which higher than the left side, 2 cases equal and 9 cases lower than the left side and this result was statistically significant ($P = 0.019$); the numbers were also lower than the ipsilateral side in the normal subjects, with the difference being statistically significant ($P = 0.024$).

Table 2 Numbers of perforating arteries detected on high-resolution 3D-TOF-MRA in heathy subjects

Perforating arteries	Left side			Right side			*P*
	Maximum	Minimum	Median	Maximum	Minimum	Median	
RAH	3	0	1	3	0	1	0.653
LSA	7	0	3	5	0	3	0.230
ACA	2	1	1	2	1	1	0.705
TPA	3	0	1	3	0	1	0.330

Wilcoxon paired test was used. $P < 0.05$ was considered statistically significant
RAH recurrent artery of Heubner; *LSA* lenticulostriate artery; *ACA* anterior choroidal artery; *TPA* thalamoperforating artery

Table 3 Comparison between 3D-TOF-MRA and CUBE T1 for detecting the LSA

	Left side	Right side	*P*
3D-TOF-MRA	3.32 ± 1.275	3.06 ± 1.209	0.230
CUBE T1	2.48 ± 1.288	2.45 ± 1.121	0.913
P	0.010	0.034	–

Wilcoxon paired test was used. $P < 0.05$ was considered statistically significant
LSA lenticulostriate artery, *3D-TOF-MRA* three-dimensional time-of-flight magnetic resonance angiography; *CUBE T1* three-dimensional fast spin-echo T1-weighted imaging

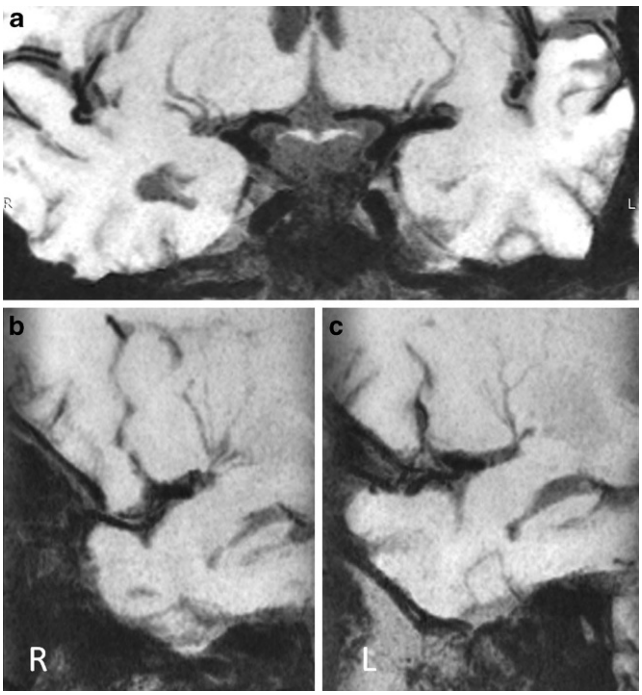

Fig. 3 Lenticulostriate arteries in normal subjects, as shown on CUBE T1. The perforating arteries showed a clear contrast with surrounding tissue with the black-blood technique on the coronal plane (**a**) and sagittal plane (**b**, **c**)

In the patients with left-sided lenticulostriate infarctions, the numbers of LSAs on the left side ranged from 0–5 (median 2) and the numbers of LSAs on the right side ranged from 1–5 (median 3). For the number of LSAs on the left side, there were 2 cases of which higher than the right side, 3 cases equal and 9 cases lower than the right side and this result was statistically significant ($P = 0.013$); the numbers were also lower than the left side in the normal subjects, with the difference being statistically significant ($P = 0.040$) (Table 4 and 5; Fig. 4).

After a further investigation, we found that there were 10 cases where the numbers of RAHs on the affected side were lower than those on the contralateral side. In addition, the difference in infarct patterns between the RAH and LSA was statistically significant ($P = 0.016$) (Table 6).

Discussion

The concept of penetrating artery disease was initially proposed by Caplan et al. [2] in 1989. They believed that deep and small infarcts may result from the occlusion of small perforating arteries with microatheroma plaques. In pathological situations these tiny arteries, which are vulnerable to hypertension, easily undergo lipohyalinosis and fibrinoid degeneration [15]. In addition, perforating arteries, such as the LSA and paramedian arteries usually arise from the trunk of major arteries at a vertical angle; impaired endothelium induced by disordered and rapid blood flow leads to the formation of atheromatous plaques. As a result, effective imaging techniques for detecting relevant pathological changes may provide valuable information in the clinical setting. In recent years, MRI has shown promise for this investigation with high-resolution imaging technology. Several ultra-high field 7 T studies have confirmed its feasibility in visualizing the cerebral perforating artery in vivo with high spatial resolution and signal-to-noise ratio, which provides not only improved vessel contrast via the longer T1 relaxation time of surrounding tissue, but also reduces the partial volume effect [16, 17]. Kang et al. [18, 19] examined the lenticulostriate arteries in a cohort of hypertensive patients using ultra-high field 7 T MRI, and

Table 4 Comparison of bilateral LSAs in the perforating artery disease group

Number	Left side			Right side			*P*
	Maximum	Minimum	Median	Maximum	Minimum	Median	
Left infarction	5	0	2	5	1	3	0.013
Right infarction	6	1	3	5	0	2	0.019

Wilcoxon paired test was used. $P<0.05$ was considered statistically significant

Table 5 Comparison of the LSA between the healthy group and disease group

Number	Affected side in disease group			Ipsilateral side in healthy group			*P*
	Maximum	Minimum	Median	Maximum	Minimum	Median	
Left infarction	5	0	2	7	0	3	0.040
Right infarction	5	0	2	5	0	3	0.024

Wilcoxon rank sum test was used. $P<0.05$ was considered statistically significant

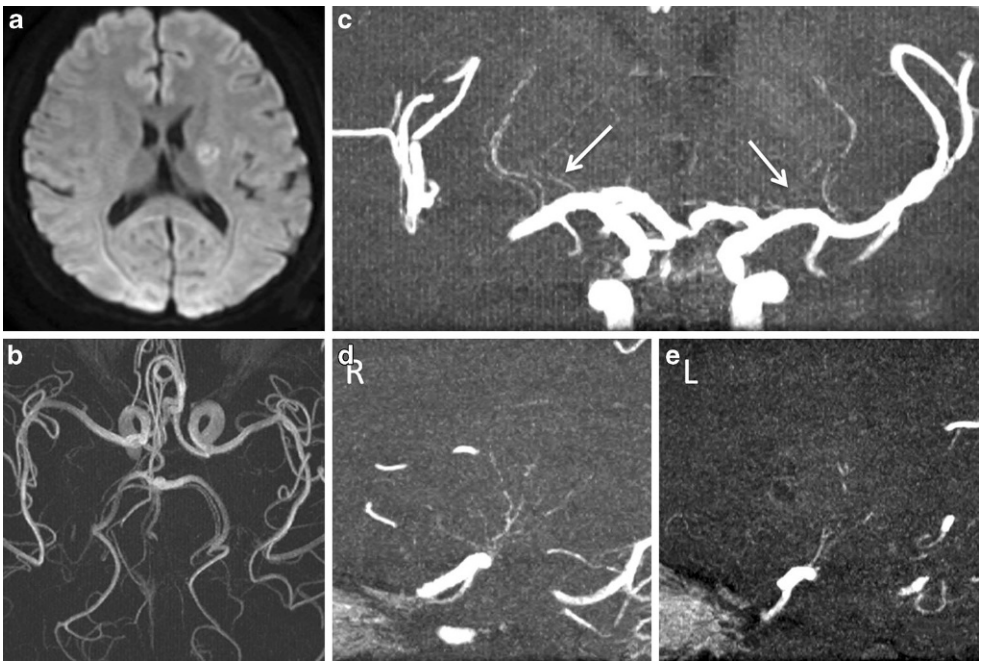

Fig. 4 A case of left basal ganglia infarction detected by DWI and HR 3D-TOF-MRA. The DWI shows a clear high signal in the left basal ganglia (**a**). No obvious stenosis or occlusion could be seen in the bilateral anterior, middle, and posterior cerebral arteries (**b**). However, the number of lenticulostriate arteries (*arrows*) on the left side was lower, and the perforating arteries appeared interrupted compared with the right side (**c**, **d**, **e**)

Table 6 Infarct patterns between RAH and LSA

Infarct pattern	LSA	RAH
Corona radiata	13 (76.5%)	2 (13.3%)
Centrum semiovale	5 (31.3%)	8 (61.5%)

LSA lenticulostriate arteries; *RAH* recurrent artery of Heubner. Data are presented as numbers (percentage)

a substantial difference was observed in the LSA of hypertensive patients compared with healthy individuals, with ultra-high field MRA providing clear anatomic delineation of the LSAs. Nevertheless, there are still several deficiencies, such as B1-field inhomogeneity as well as the need for development of special radiofrequency coils. Moreover, the specific absorption rate will significantly increase on such a high field MR scanner [19]. Notably, 7 T MRI is still not widely used or available in most hospitals. As a result, a 3 T MR scanner may be more suitable for a clinical application in the diagnosis of perforating artery disease. In our study, the spatial resolution and signal-to-noise ratio on a 3 T MR scanner were adequate for showing the perforating artery with satisfactory results.

Display of Perforating Arteries in Normal Subjects

Anatomically, the diameter of the extracranial RAH is 662–1000 μm and its terminal branches measure approximately 462 μm in diameter [20, 21]. The number of LSAs is inversely proportional to the diameter of the vessel and its diameter at the initial site is 100–2200 μm [22, 23]. The diameter of the ACA at the initial site is 0.7–2.0 mm, with the average being 1.2 mm [24]. The number of TPAs ranges from 1–10, with an average number of 2, the diameter of the extracranial segment is 100–750 μm, with an average

of 321 μm [25]. In this study, we used HR 3D-TOF-MRA to observe the perforating arteries in normal subjects. The voxel was as small as 0.48 mm × 0.40 mm × 0.6 mm, providing the possibility to visualize the perforating arteries. Whole segments of most of the perforating arteries, from the beginning to the terminus of each, were clearly shown with high signal on HR 3D-TOF-MRA, except for some perforating arteries from the posterior circulation. There were two reasons accounting for this limitation. The diameter of the initial or distal segment of the perforating artery is too small to be detected under the current imaging voxel of our HR sequence. In contrast, if the flow is perpendicular or nearly perpendicular to the scan plane and the TR is too short, the protons in the scan plane do not have sufficient time for complete longitudinal relaxation, resulting in signal attenuation and poor detection of these arteries [26]. The voxel of CUBE T1 is 0.48 mm × 0.57 mm × 0.6 mm. With the advantages of black blood, fat suppression, multiplanar reconstruction, and insensitivity of flow direction, CUBE T1 may show superiority in visualizing the pathological changes in the vessel walls, whereas HR 3D-TOF-MRA may specialize in detecting the number of perforating arteries with the bright blood technique and higher resolution contrast to CUBE T1.

Display of the Perforating Arteries in the Perforating Arteries Disease Group

In this study, we found that the number of LSAs on the affected side in most patients was lower compared with the contralateral side and normal subjects, suggesting a reason for deep infarcts. This may have resulted from occlusion by the atherosclerotic plaques originating from the large artery at the opening of the perforating arteries [27]. There were nine patients with a history of hypertension and six patients with diabetes included in our study, both of which diseases are high-risk factors in small artery disease. These patients can show acute progression from symptom onset to infarction detected by DWI. The HR-MRI also showed a thickened vessel wall and plaque at the proximal segment of the MCA. In a small number of patients, no statistically significant differences in number were found between both sides of the LSA; however, the distal segments of the LSA in the infarcted area were either not developed or intermittently developed, and the vessel walls became coarse, which may account for the pathological changes of lipohyalinosis and fibrinoid degeneration occurring in the culprit arteries. Hypertension was also found in some of these patients and they had subacute symptoms as the blood supply did not decrease dramatically. There were three patients with high low-density lipoprotein levels manifesting with hyperacute symptoms and large lesions in the LSA territory after symptom onset. The HR-MRI showed a normal MCA and an incomplete segment of LSA, which may have resulted from the obstruction of the only perforating artery by remote microemboli. There was still a minority of patients in whom contradictory results in numbers between the affected side and contralateral side of the LSA were found. The reasons may have accounted for individual differences**;** the numbers of LSAs on both sides were not equal before infarction, or there may have been a technical limitation**.** The diameter at the initial or distal segment of the LSA was too small to be detected under the current resolution of 3D-TOF-MRA used in this study.

The RAH is normally the largest of the medial LSA branching from the proximal A2 or A1 segment of the ACA. It generally supplies the anteromedial part of the caudate nucleus, the anterior limb of the internal capsule, the anterior third of the putamen, and the globus pallidus [28]. The LSA sprouts vertically from the MCA and primarily supplies the upper part of the head and the body of the caudate nucleus, the putamen, the lateral part of the pallidum, the superior part of the anterior and posterior limbs, and the genu of the internal capsule [3]. In this study, significant differences in the infarct patterns were observed between the RAH and LSA. Abnormality of the RAH may have led to a higher plane infarct in the centrum semiovale, whereas an abnormality of the LSA was related to a lower plane infarct in the corona radiata. The clinical symptoms were also different. The patients may develop dysarthria, nonpyramidal hemimotor dysfunction, and behavioral and cognitive abnormalities when the RAH is involved, or they primarily manifest as dyskinesia such as hemiplegia when the LSA is involved. The infarct patterns may help to further distinguish their stroke mechanisms in perforating artery disease.

The HR 3D-TOF-MRA showed that there were at least three fixed LSAs with clear borders in the normal subjects. We can infer the cause of perforating artery disease according to the number and morphological changes of the focal perforating arteries; however, the imaging was unable to detect the signal changes within the vessel walls and inside the lumen for a strict distinction of proximal atherosclerosis from distal lipohyalinosis, which were always concomitant. Moreover, few people die from the small infarctions occurring in the perforating arteries; therefore, there is limited pathological evidence because few autopsies were carried out in these patients. With the development of imaging technology, it is believed that the two pathological mechanisms of perforating artery disease will be recognized, which is helpful for further classification of stroke subtypes and the identification of their etiology, as well as for risk stratification.

In addition to the deficiencies mentioned above, there were other limitations in our study. First, because the technique of TOF is based on the influx enhancement effect of blood flow, HR 3D-TOF-MRA is susceptible to the velocity

of blood flow, which we have not accounted for between the different age stages [29]. In a future study, we will divide the healthy subjects into different age groups and evaluate the ability of HR 3D-TOF-MRA to detect the perforating arteries at different age stages. Second, although we used some techniques to reduce the scan time, two HR sequences were conducted over nearly 20 min, which was inappropriate for the acute patients. In addition, the long scan time increases motion artifacts. Third, we only compared the number of LSAs and RAHs in the deep infarcts of the basal ganglia; whether there were other perforating arteries supplying the same territory was not explored. Fourth, the number of perforating arteries varied greatly from person to person [30]. The results may be contradictory in research using a small sample size. We are cautious about interpreting the results of the infarct pattern in this study as the sample size is still not large enough. A large sample size is needed to validate the use of the infarct pattern in the identification of the stroke mechanism in the future.

Conclusion

In summary, HR-MRI plays an important role in the detection of the tiny perforating arteries in vivo. The CUBE T1 technique may showed superiority in visualizing the pathological changes in the vessel walls whereas HR 3D-TOF-MRA may specialize in detecting the number of perforating arteries. In addition, these sequences may help in the identification of arteries presumably causing deep infarcts and heterogeneous infarct patterns.

Funding This work was supported by Collaborative Innovation Program of Hong Kong and Guangdong Province (grant numbers 2016A050503032).

Conflict of interest J. Liang, Y. Liu, X. Xu, C. Shi and L. Luo declare that they have no competing interests.

References

1. Yang G, Wang Y, Zeng Y, Gao GF, Liang X, Zhou M, Wan X, Yu S, Jiang Y, Naghavi M, Vos T, Wang H, Lopez AD, Murray CJ. Rapid health transition in China, 1990–2010: findings from the global burden of disease study 2010. Lancet. 2013;381:1987–2015.
2. Caplan LR. Intracranial branch atheromatous disease: a neglected, understudied, and underused concept. Neurology. 1989;39:1246–50.
3. Decavel P, Vuillier F, Moulin T. Lenticulostriate infarction. Front Neurol Neurosci. 2012;30:115–9.
4. Bodle JD, Feldmann E, Swartz RH, Rumboldt Z, Brown T, Turan TN. High-resolution magnetic resonance imaging: an emerging tool for evaluating intracranial arterial disease. Stroke. 2013;44:287–92.
5. Li M, Le WJ, Tao XF, Li MH, Li YH, Qu N. Advantage in bright-blood and black-blood magnetic resonance imaging with high-resolution for analysis of carotid atherosclerotic plaques. Chin Med J. 2015;128:2478–84.
6. Bykanov AE, Pitskhelauri DI, Pronin IN, Tonoyan AS, Kornienko VN, Zakharova NE, Turkin AM, Sanikidze AZ, Shkarubo MA, Shkatova AM, Shults EI. 3D-TOF MR-angiography with high spatial resolution for surgical planning in insular lobe gliomas. Zh Vopr Neirokhir Im N N Burdenko. 2015;79:5–14.
7. Rao AS, Thakar S, Sai Kiran NA, Aryan S, Mohan D, Hegde AS. Analogous three-dimensional constructive interference in steady state sequences enhance the utility of three-dimensional time of flight magnetic resonance Angiography in delineating Lenticulostriate arteries in insular Gliomas: evidence from a prospective Clinicoradiologic analysis of 48 patients. World Neurosurg. 2018;109:e426–33.
8. Li ML, Xu YY, Hou B, Sun ZY, Zhou HL, Jin ZY, Feng F, Xu WH. High-resolution intracranial vessel wall imaging using 3D CUBE T1 weighted sequence. Eur J Radiol. 2016;85:803–7.
9. Yang H, Zhu Y, Geng Z, Li C, Zhou L, Liu QI. Clinical value of black-blood high-resolution magnetic resonance imaging for intracranial atherosclerotic plaques. Exp Ther Med. 2015;10:231–6.
10. Zhao DL, Deng G, Xie B, Ju S, Yang M, Chen XH, Teng GJ. High-resolution MRI of the vessel wall in patients with symptomatic atherosclerotic stenosis of the middle cerebral artery. J Clin Neurosci. 2015;22:700–4.
11. Xu P, Lv L, Li S, Ge H, Rong Y, Hu C, Xu K. Use of high-resolution 3.0-T magnetic resonance imaging to characterize atherosclerotic plaques in patients with cerebral infarction. Exp Ther Med. 2015;10:2424–8.
12. Yamamoto Y, Nagakane Y, Tomii Y, Toda S, Akiguchi I. The relationship between progressive motor deficits and lesion location in patients with single infarction in the lenticulostriate artery territory. J Neurol. 2017;264:1381–7.
13. Wang Y, Wang J. Clinical and imaging features in different inner border-zone infarct patterns. Int J Neurosci. 2015;125:208–12.
14. Edjlali M, Roca P, Rabrait C, Naggara O, Oppenheim C. 3D fast spin-echo T1 black-blood imaging for the diagnosis of cervical artery dissection. AJNR Am J Neuroradiol. 2013;34:E103–E6.
15. Andrade MR, Pittella JE. Immunohistochemical identification of plasma protein deposits in the wall of lenticulostriate arteries in patients with long-standing hypertension, with and without lipohyalinosis. Arq Neuropsiquiatr. 2009;67:82–9.
16. Harteveld AA, De Cocker LJ, Dieleman N, van der Kolk AG, Zwanenburg JJ, Robe PA, Luijten PR, Hendrikse J. High-resolution postcontrast time-of-flight MR angiography of intracranial perforators at 7.0 T. PLoS One. 2015;10:e121051.
17. Seo SW, Kang CK, Kim SH, Yoon DS, Liao W, Wörz S, Rohr K, Kim YB, Na DL, Cho ZH. Measurements of lenticulostriate arteries using 7 T MRI: new imaging markers for subcortical vascular dementia. J Neurol Sci. 2012;322:200–5.
18. Kang CK, Park CA, Lee H, Kim SH, Park CW, Kim YB, Cho ZH. Hypertension correlates with lenticulostriate arteries visualized by 7 T magnetic resonance angiography. Hypertension. 2009;54:1050–6.
19. Kang CK, Park CW, Han JY, Kim SH, Park CA, Kim KN, Hong SM, Kim YB, Lee KH, Cho ZH. Imaging and analysis of lenticulostriate arteries using 7.0-Tesla magnetic resonance angiography. Magn Reson Med. 2009;61:136–44.
20. Gomes F, Dujovny M, Umansky F, Ausman JI, Diaz FG, Ray WJ, Mirchandani HG. Microsurgical anatomy of the recurrent artery of Heubner. J Neurosurg. 1984;60:130–9.
21. Marinković S, Milisavljević M, Kovacević M. Anatomical bases for surgical approach to the initial segment of the anterior cerebral artery. Microanatomy of Heubner's artery and perforating branches of the anterior cerebral artery. Surg Radiol Anat. 1986;8:7–18.
22. Herman LH, Ostrowski AZ, Gurdjian ES. Perforating branches of the middle cerebral artery. An anatomical study. Arch Neurol. 1963;8:32–4.

23. Marinković S, Gibo H, Milisavljević M, Djulejić V, Jovanović VT. Microanatomy of the intrachoroidal vasculature of the lateral ventricle. Neurosurgery. 2005;57(1 Suppl):22–36. discussion 22–36.
24. Rhoton AL Jr., Fujii K, Fradd B. Microsurgical anatomy of the anterior choroidal artery. Surg Neurol. 1979;12:171–87.
25. Marinković S, Milisavljević M, Kovacević M. Interpeduncular perforating branches of the posterior cerebral artery. Microsurgical anatomy of their extracerebral and intracerebral segments. Surg Neurol. 1986;26:349–59.
26. Grochowski C, Staśkiewicz G. Ultra high field TOF-MRA: A method to visualize small cerebral vessels. 7T TOF-MRA sequence parameters on different MRI scanners—Literature review. Neurol Neurochir Pol. 2017;51:411–8.
27. Bae YJ, Choi BS, Jung C, Yoon YH, Sunwoo L, Bae HJ, Kim JH. Differentiation of deep subcortical infarction using high-resolution vessel wall MR imaging of middle cerebral artery. Korean J Radiol. 2017;18:964–72.
28. Maga P, Tomaszewski KA, Skrzat J, Tomaszewska IM, Iskra T, Pasternak A, Walocha JA. Microanatomical study of the recurrent artery of Heubner. Ann Anat. 2013;195:342–50.
29. Li W, Xu F, Schär M, Liu J, Shin T, Zhao Y, van Zijl PCM, Wasserman BA, Qiao Y, Qin Q. Whole-brain arteriography and venography: using improved velocity-selective saturation pulse trains. Magn Reson Med. 2018;79:2014–23.
30. Kammerer S, Mueller-Eschner M, Berkefeld J, Tritt S. Time-resolved 3D rotational Angiography (4D DSA) of the lenticulostriate arteries: display of normal anatomic variants and collaterals in cases with chronic obstruction of the MCA. Clin Neuroradiol. 2017;27:451–7.